FINDINGS: CAST MODULAR NODES FOR SEISMIC RESISTANT STEEL FRAMES

This interim report contains an update of the findings made on NSF **CMS 01-96120** to the time period ending May 31, 2002. The report is organized according to connection concept: (A) Modular Connector; and, (B) Modular Node.

A. MODULAR SEMI-RIGID CONNECTOR FOR PRF'S

A.1. ANALYTICAL RESULTS

The analytical program involved three main studies: (A) general behaviour; (B) parametric study; and (C) a comparison of the MC to an analogous traditional tee-stub connection.

A.1.a ANALYTICAL RESULTS:GENERAL BEHAVIOR

Prior to presenting the parametric study results (Section A.1.b), results are given indicating the general behavior. In section 5A general behaviour of the MC end-region configurations are presented. In Section 5B, the MC is compared to a constant width plate and the ADAS geometry. In section 5C, MC Arm basic properties are decsribed.

A.1.a.1 End-Region: General Behavior

MCnobase, MCoutrigger, MCeccentric, MCbase have very similar overall load deflection behavior. The MC arm performance is satisfactory in each configurations. The column bolt performance heavily depends on the end-region configuration. Due to different end-region configurations, each MC model has different catenary force demands (See Fig. 1). When the catenary force demand reaches the amount of frictional force due to pretensioning of the bolt, end region starts sliding. The bolt head moves with the end region. Therefore, the transverse displacement of the bolt head puts an additional amount of moment to the bolt in double curvature. The bolt shank hits the column flange in later displacement demand stages. Bearing of the bolt to the column flange introduces a new boundary for the bolt which shortens the effective flexural length of the bolt. Therefore this action increases the flexural stiffness of the bolt. Greater stiffness of the bolt attracts more catenary forces. Additional amount of catenary forces are resisted by the bolt shank. Shear failure occurs at the later stages.

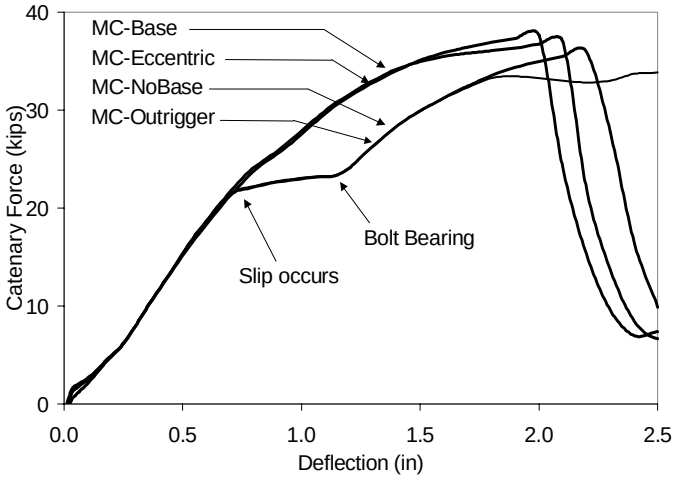

Figure 1. The catenary force in the MC arm.

A.1.a.2 MC Arm Geometry

At high transverse displacement demands, concentration of plastic strain is observed at the ends of the plate and at the middle of the ADAS device (See Figure 2 and 3). A relatively uniform plastic distribution in the arm of MC is obtained. The ratios, (B_{min}/B_{max}) = 0.45, (L/B_{max}) = 2, shown later to be optimum (See Section A.1.b), are used. Figure 8 is representative of all MCs of practical length.

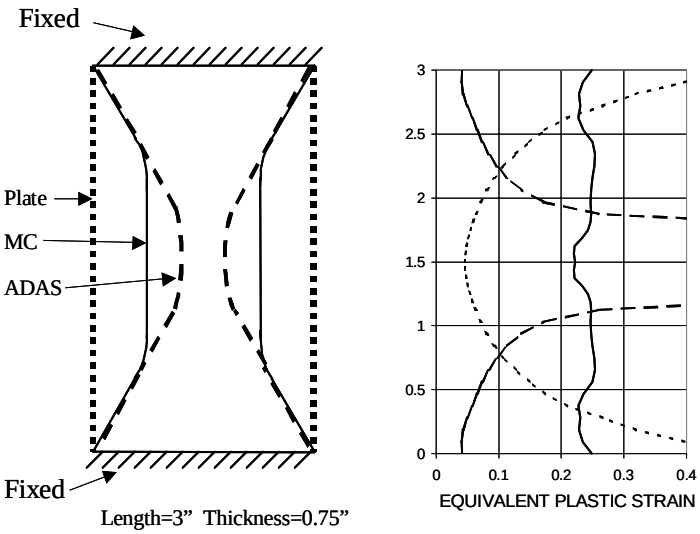

Figure 2. Equivalent plastic strain distribution (0.05rad for 30" beam).

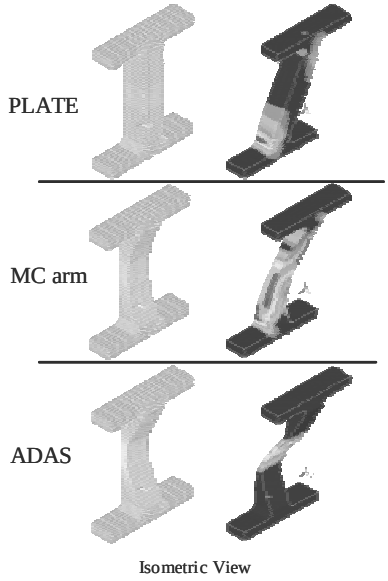

Figure 3. Distribution of equivalent plastic strain in plate, MC arm and ADAS (0.05rad for 30" beam)

A.1.a.3 MC Arm Basic Properties

The following evaluations are obtained from the results of the parametric study: (A) Evaluated designs of constant strength; (B) Overstrength evaluation; and, (C) Stability point evaluation. Design charts that contain yield and ultimate strength of the MC are presented to the reader in the following sections.

A.1.a.3.1 Strength

Yield strength (P_y) and ultimate strength (P_u) of connector depend on geometry of the arm. The yield value is related to the maximum width of the arm; the ultimate value is related to the minimum width. Figure 4 indicates that for a constant t, L and B_{max}, P_u depends on B_{min}.

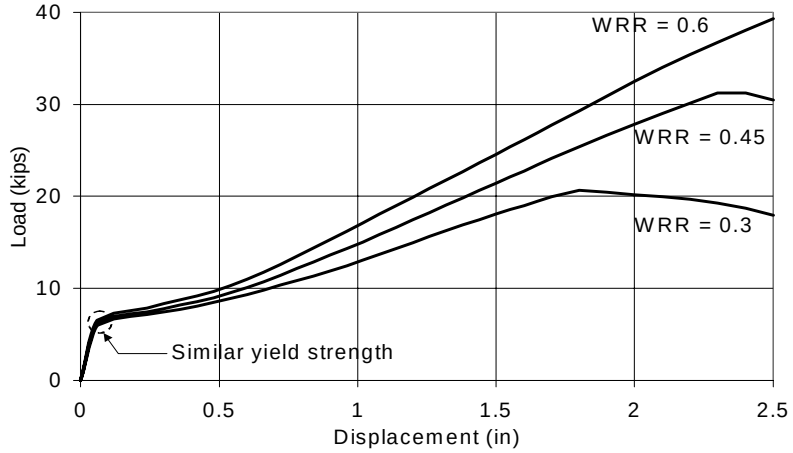

Figure 4. Load displacement of the MC arm for various width reduction ratio (WRR) [L = 5in, t = 0.75in, B_{max}= 2.5in].

Equation 5 implies that for a constant L/B_{max} ratio, the P_y depends on the arm thickness alone. In other words, P_y can be used to select the thicknesss. The MC arm yield and useable strength versus thicknesses is shown in Figure 5. P_u versus length for various thicknesses is shown Figure 6.

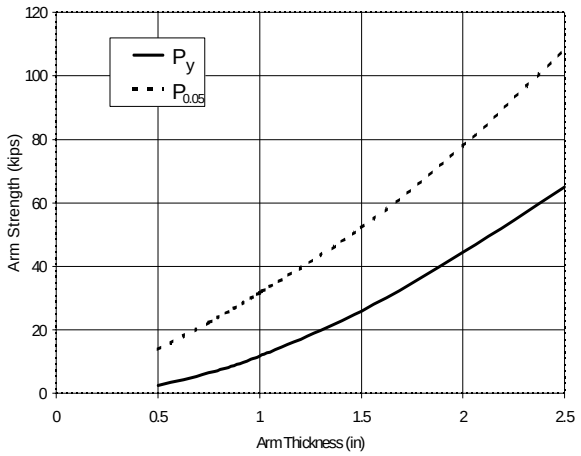

Figure 5. Strength of the MC arm at different displacement demands for various thicknesses

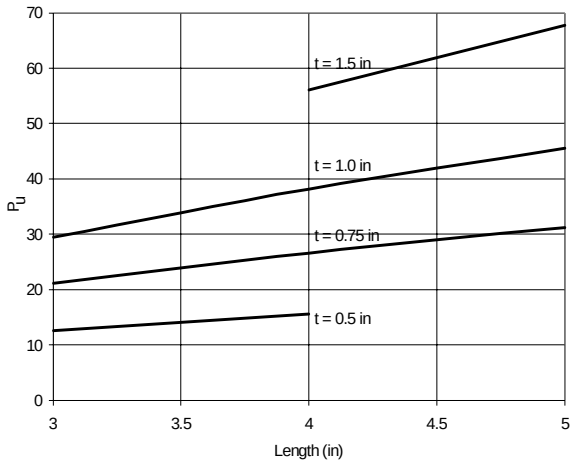

Figure 6. Ultimate Strength of MC arms for various thicknesses

A.1.a.3.2 Ductility

Figure 7 indicates that for optimum arm geometry ratios, longer arm produces a lower ductility demand. For a specified ductility demand, MC arms with different lengths and thicknesses can be chosen (See point A, A' and A" in Figure 7)

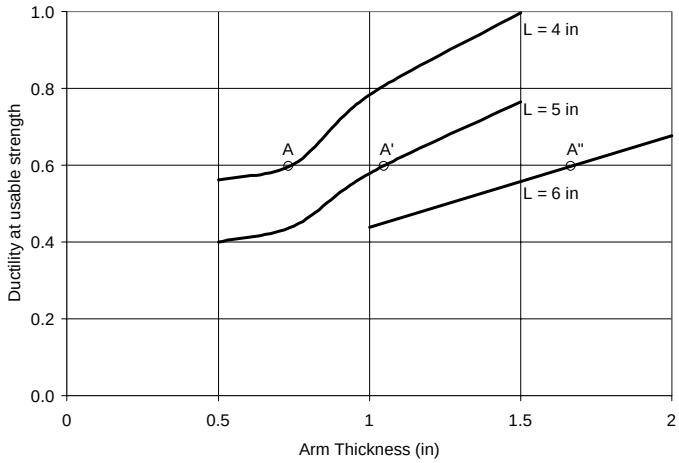

Figure 7. Ductility of MC arm at usable strength

A.1.a.1.3 Stability Point

The longer the arm, the more deflection occurs before reaching the load-deflection stability point. Axial stiffness (AE/L) strongly affects the catenary force. The thicker the arm, the greater the Δ_u. For the MC optimum geometry, the effect is not strong because an increase in A_{crit} is accompanied by an increase in M_p.

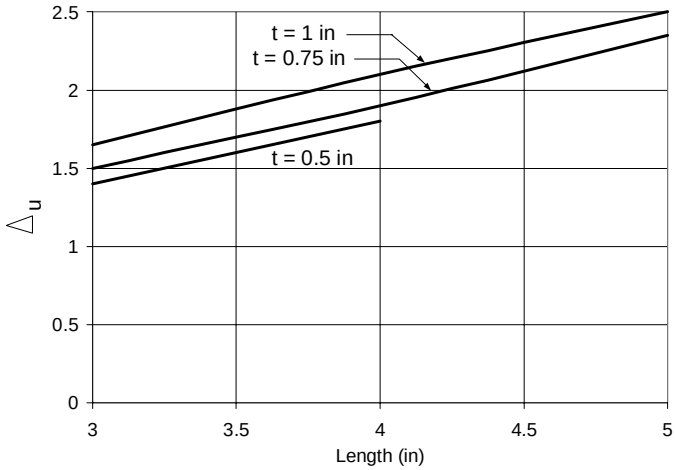

Figure 8. Load deflection stability points for various MC arm lengths and thicknesses.

A.1.a.3.4 Overstrength

Equation 5 (See progress report) implies that, the yield strength of an MC arm is directly related to the second power of the arm thickness. Equation 6 (See progress report) implies that,

the ultimate strength is directly related to the thickness. Therefore, as the thickness increases, the overstrength decreases. (See Figure 9 and 10).

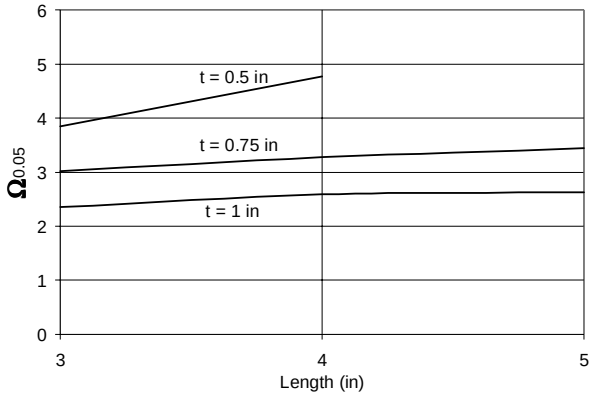

Figure 9. Overstrength of the MC arm at 0.05rad.

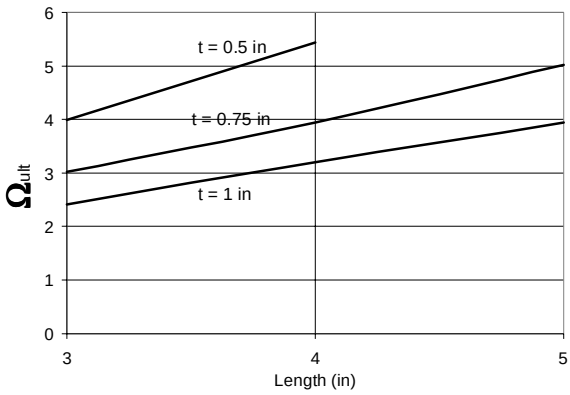

Figure 10. Overstrength of the MC arm at stability point.

A.1.b ANALYTICAL RESULTS: PARAMETRIC STUDY

A detailed parametric study was performed to isolate effects of different dimensions on the behavior of the hourglass arm. The following parameters describing the MC arm are examined: (1) Fillet Radius; (2) Width Reduction Ratio; (3) Length to Width Ratio; and, (4) Effect of Length and Thickness.

A.1.b.1 Fillet Radius

The fillet radius (r_0) producing the minimum value of ε_{arm}^{pl} at each length was selected as optimal and used for the MC. r_0 seems more critical for shorter lengths (See Figure 11). The fillet plays an important role at high strain demands. Very small fillet radii create a location of concentrated plastic strain demand.

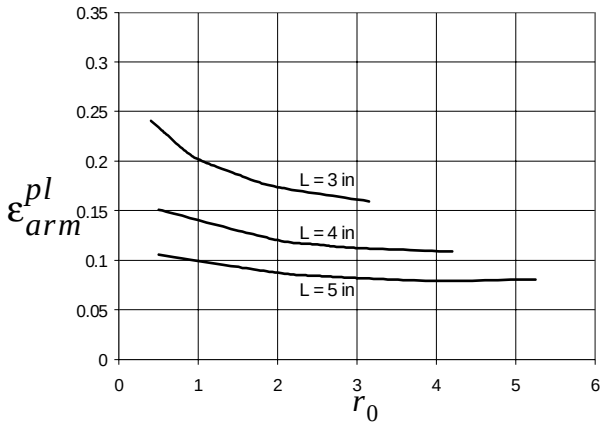

Figure 11. r_0 vs. ε_{arm}^{pl} at 0.03rad

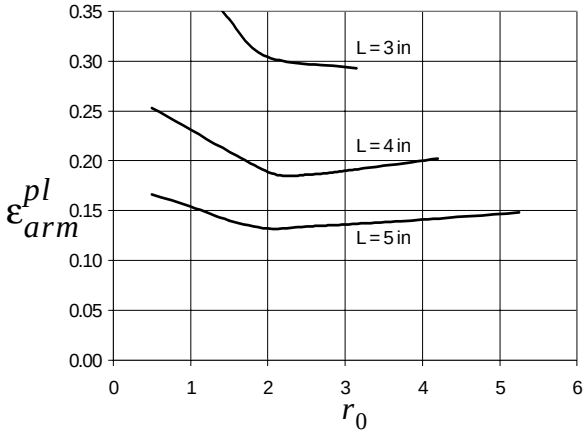

Figure 12. r_0 vs. ε_{arm}^{pl} at 0.05 rad

A.1.b.2 Width Reduction Ratio:

Figure 13 implies performances of MC arms with different width reduction ratios for constant t and L/B_{max} . A ratio of 0.45 was selected as an optimum ratio in MC (See Figure 13).

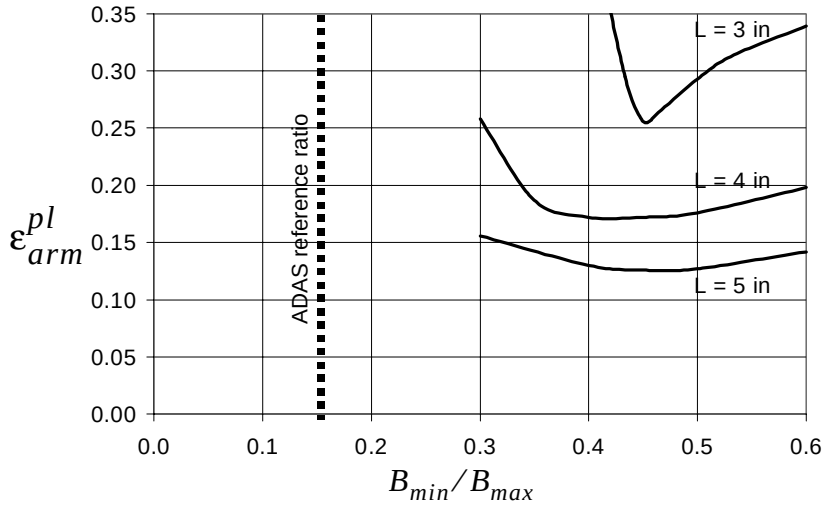

Figure 13. Width reduction ratio versus ε_{arm}^{pl} for various lengths at useable streng

A.1.b.3 Length-To-Width:

Length-to-width study investigates the effect of varying the width for a given arm length, thickness and width reduction ratio. As seen in Figure 14, as L/B_{max} increases, ε_{arm}^{pl} decreases. For $L/B_{max}>1.75$, ε_{arm}^{pl} reaches a level at which it does not decrease further. From a practical standpoint, L/B_{max} controls the number of arms in a connector. Note that, for casting point of view, it is better to use minimum amount of arms within a connector. Therefore, a ratio of 2.0 was

selected as an optimum number for the MC arm (See Figure 14). A ratio of approximately 2.0 is used in the ADAS device.

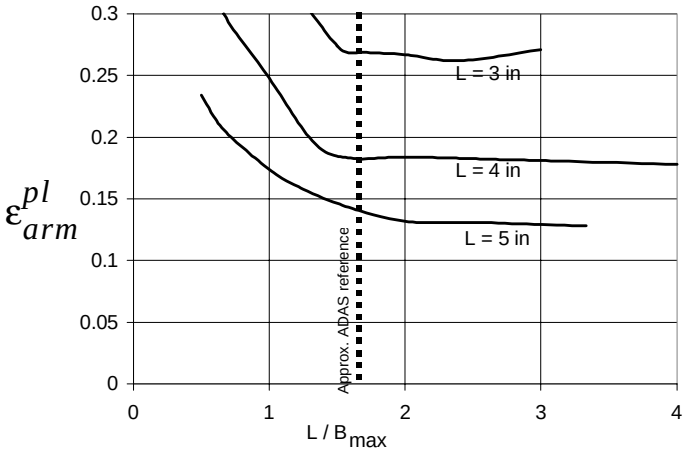

Figure 14. ε_{arm}^{pl} versus L/B_{max} (t = 0.75in.).

A.1.b.4 Effect of Length and Thickness:

The effect of length, thickness and their relative values is examined. In the first examination, a "stretch" study, the arm length is varied while the arm width and thickness are kept constant (See Figure 15a). The study is performed at maximum widths of 1.5, 2, 2.5 inches. As implied in Figure 15b, the rate of decrease of the maximum plastic strain is greater than that of the yield strength, thus the net effect is slightly more efficient as the length of the arm increases. The efficiency of the arm may be indicated in terms of an index called alpha (See Equation 7, Progress Report).

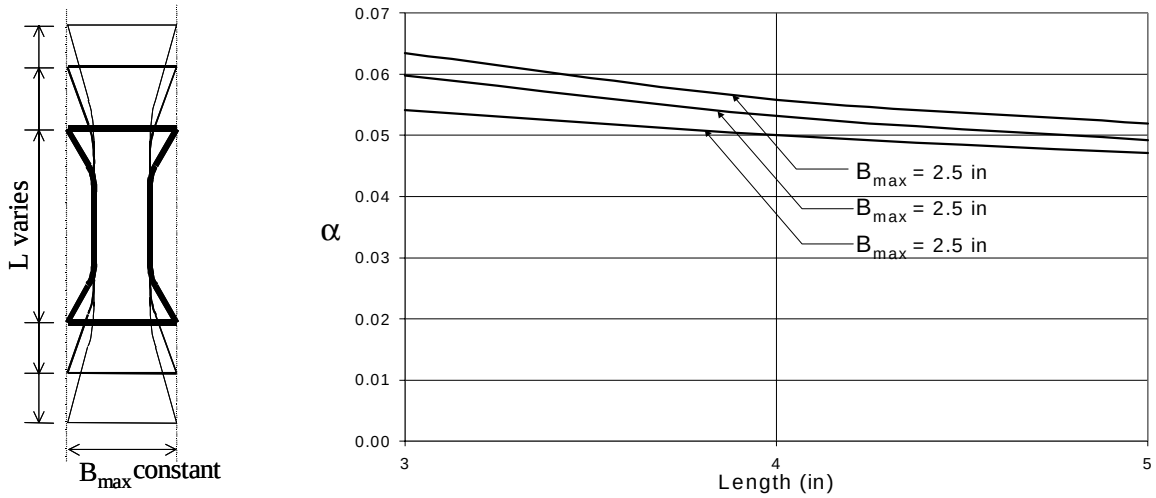

(a) **(b)**

Figure 15. (a) Schematic of "Stretch" study; (b) Length versus alpha. (t=0.75 in)

In the second examination, MC arms of similar strength are evaluated for different lengths. In the study, L/B_{max} and t are held constant. ε_{arm}^{pl} decreases considerably with an increase in the length. As the length increases, the strength and the stiffness decreases. However, a longer arm may be a better design because, α value still goes down (See Figure 16).

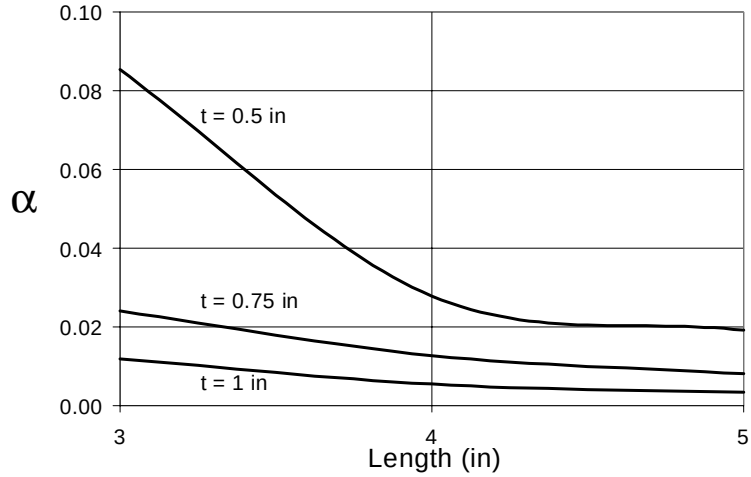

Figure 16. Effect of length study.

The effect of thickness is examined next. In the analyses, width reduction ratio and L/B_{max} are kept constant. The rate of the strength increase is higher than ε_{arm}^{pl} , it can be concluded that a thicker arm represents a more efficient design (See Figure 17).

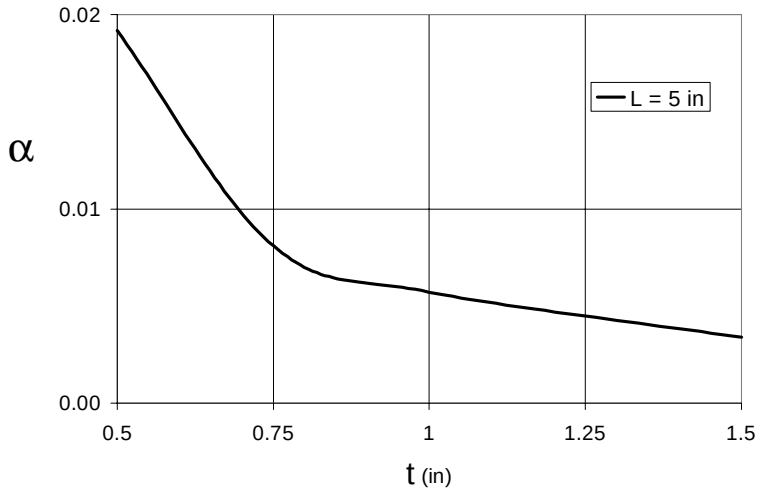

Figure 17. Effect of thickness.

A.1.c COMPARISON TO TEE-STUB

Figures 18 and 19 show FE models of the tee-stub detail piece and the MC of similar strength and stiffness. Equivalent plastic strain is shown in the contours at the identical deformation demand (0.067 rad for a W30 beam).

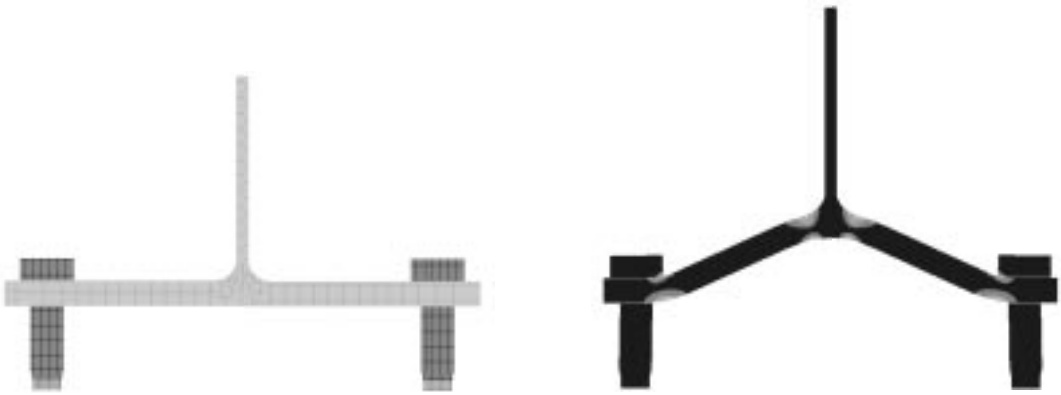

Figure 18. (a) FE model WT 7x49.5 (b) Equivalent plastic strain distribution WT 7x49.5 at 0.067rad

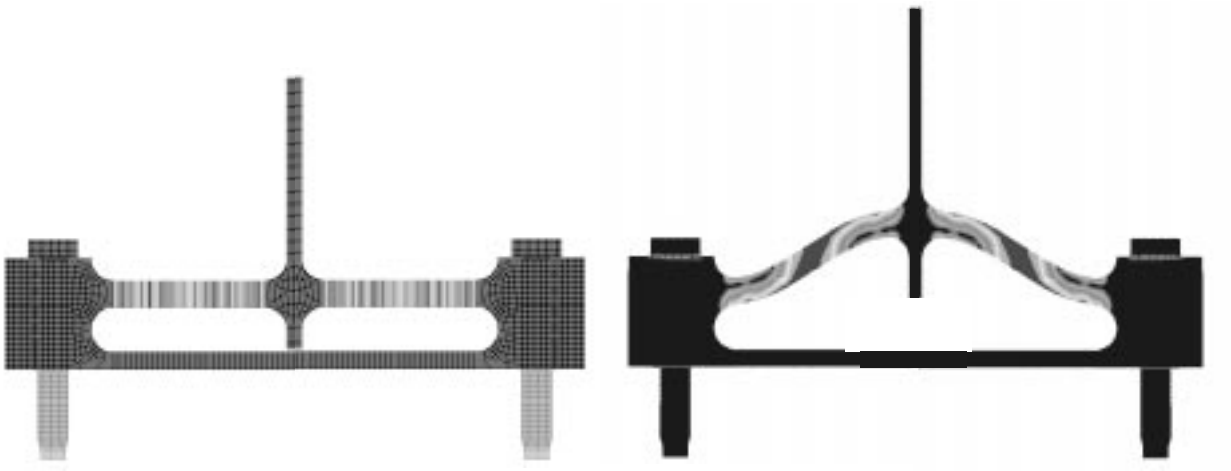

Figure 19. (a) FE model the MC (b) Equivalent plastic strain distribution MC at 0.067rad

The load displacement plot is shown for the MC and the tee-stub (See Figure 20). This plot indicates that the MC and tee-stub are nominally similar in stiffness and strength; however the MC does achieve greater secondary strength. This reserve strength occurs due to a more sig-

nificant presence of the catenary action.

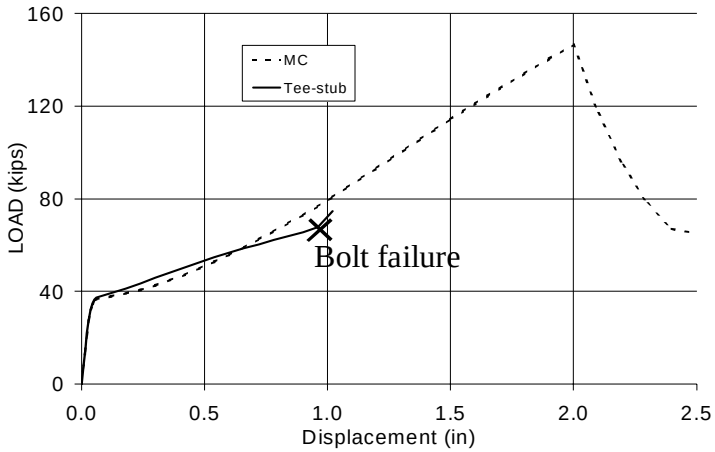

Figure 20. Load vs. deflection of the MC and the tee-stub.

In comparison to the tee-stub, the MC exhibits: (1) significantly lower plastic strain in the bolt threads; (2) no plastic behavior in the bolt shank; and, (3) lower plastic strain in the detail piece (See Figure 21 and 22).

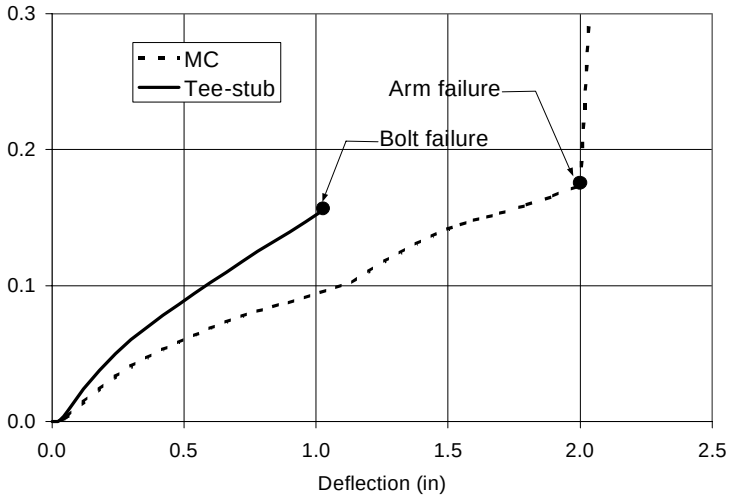

Figure 21. ε_{arm}^{pl} comparison of the MC arm and tee-stub arm.

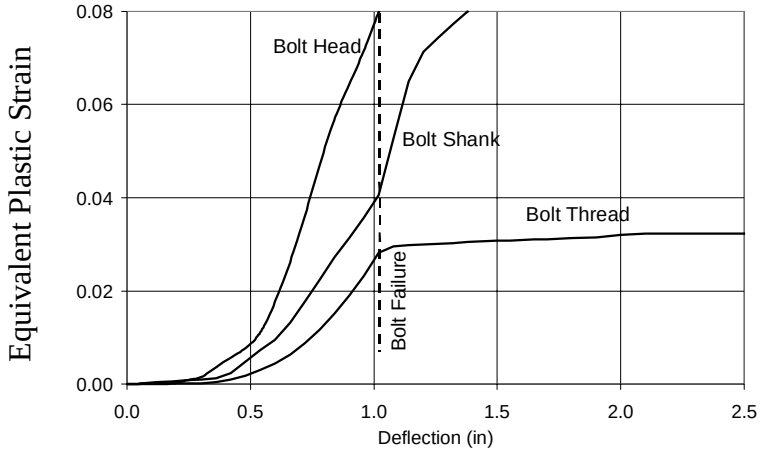

Figure 22. Bolt equivalent plastic strain versus deflection of the tee-stub connection at the bolt shank, thread, and the head.

In Figure 23, higher catenary forces are observed in the MC than the tee-stub. The tee-sub configuration permits displacement of the arms after bolt slip and subsequent hole ovalization or bolt shearing. The MC does not allow any slippage or shearing of the bolt, and thus generates the catenary forces.

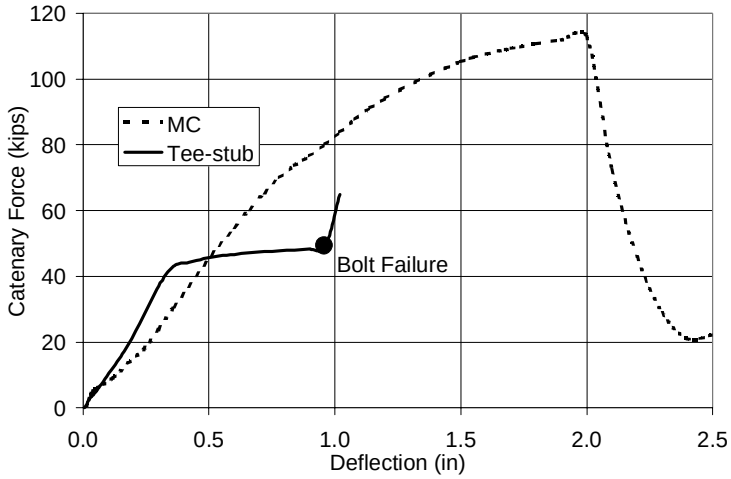

Figure 23. Comparison of catenary forces in the arm of the MC and the tee-stub.

A.1.d PREDICTION MODELS

A.1.d.1 Stability Point Prediction

Critical axial force ($N_{critical}$) is defined as the axial force capacity of the MC arm.

$$N_{critical} = 0.904(t)(B_{min})(\sigma_u) \tag{8}$$

The stability point is predicted by formula shown below (See Figure 24).

$$\Delta_u = 0.4855(t)^{0.25}(L) \tag{9}$$

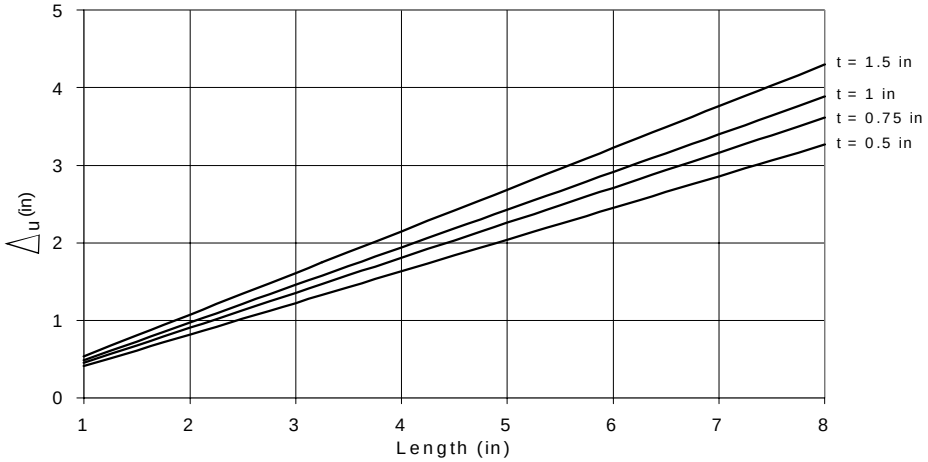

Figure 24. Stability point prediction

A.1.d.2 Ultimate Strength Prediction

The ultimate strength of the arm depends on the yield strength, minimum cross sectional area, the length and the thickness of the arm. It can be approximated as follows:

$$P_u = P_y + N_{critical}\left[\cos\left(\operatorname{atan}\left(\frac{L}{\Delta_u}\right)\right)\right] \tag{10}$$

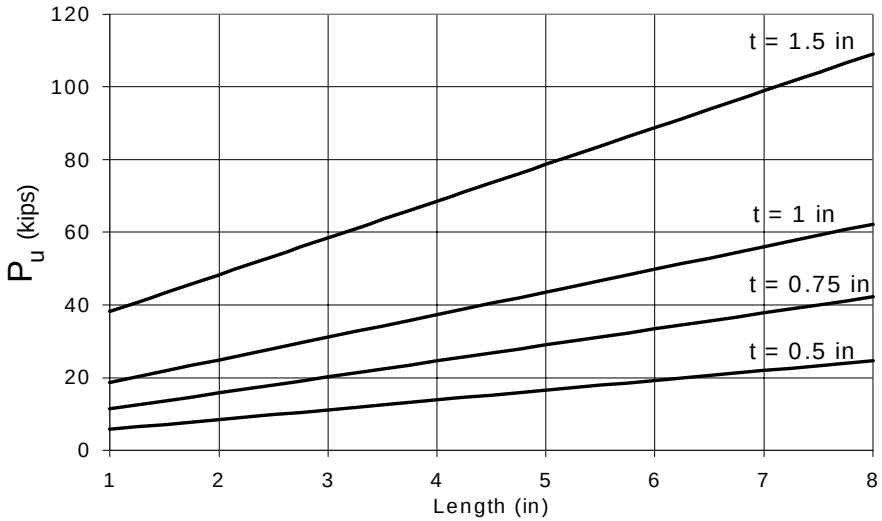

Figure 25. Prediction of the ultimate strength of the arm for various thicknesses.

A.1.d.3 Overstrength Prediction

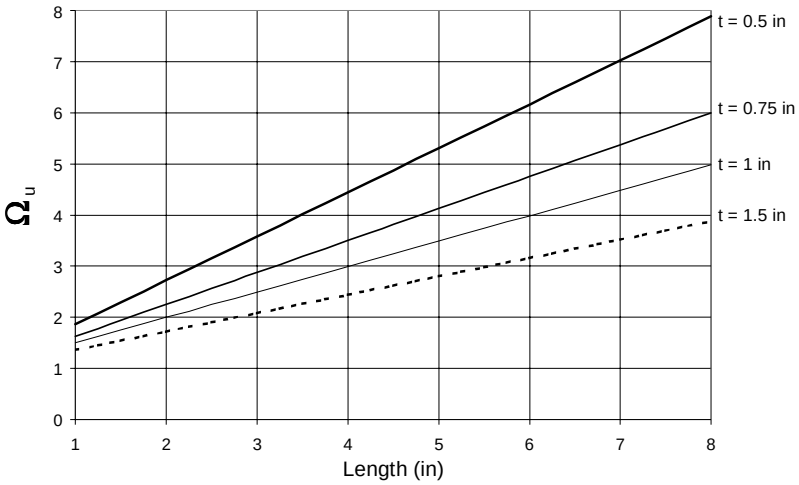

Figure 26. Analytical prediction of the MC arm overstrength ratio.

A.2 EXPERIMENTAL RESULTS

Experimental program consisted of two stages (A) pilot tests: 4 MC Base and 2 MC No Base (B) 4 full-scale beam-column tests to be tested individually under cyclic and monotonic loads. Only the pilot tests are addresses in this report.

A.2.a MC-Base

Figure 27 shows a force-deformation curve of MC-Base tested monotonically. FE results shows good agreement with the experimental results. In this case, a rotation of 0.1 rad can be approximated for a W24 beam. Figure 28 shows a load-deformation curve of MC-Base tested cyclically. Notice that the deformations are larger in tension than in compression as a result of the testing procedure discussed previously (See Proggress Report). In the cyclic test case, a rotation of 0.083 rad can be approximated for a W24 beam from peak to peak displacement of about 2.0 inches.

Figure 27. MC-Base

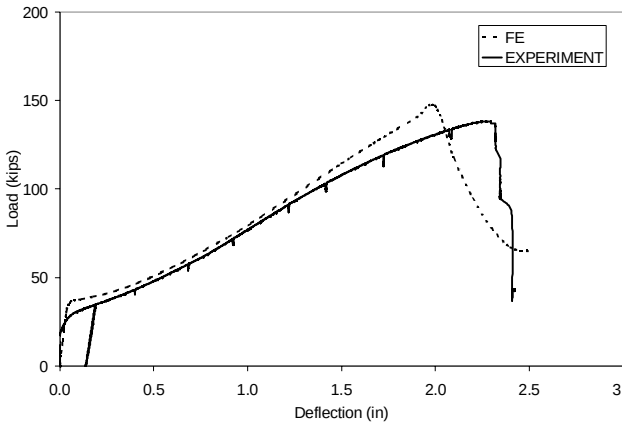

Figure 28. Load Deflection comparison

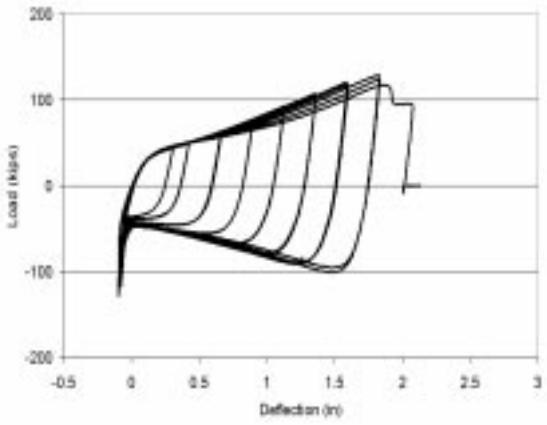

Figure 29. MC-Base under cyclic loading

MC-Base did exhibit the desired spread of plasticity engineered into the MC. 10 strain gages located on the MC arm permitted the observation of the distribution of the plasticity spread throughout the MC arms. Prior to testing, MC was whitewashed. Figure 30 shows the spread of plasticity.

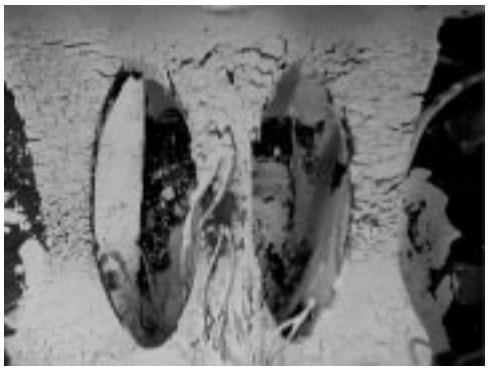

Figure 30. Spread of plastic region in MC

A comparison of the FE model and experimental results for a representative MC arm is shown in Figure 31.

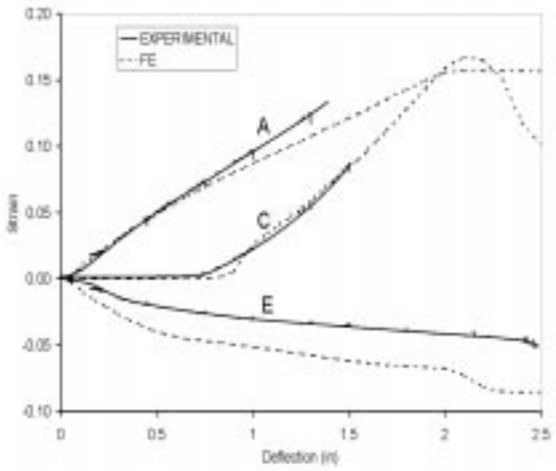

Figure 31. Strain demand in MC-Base arm. FE versus Monotonic Behaviour.

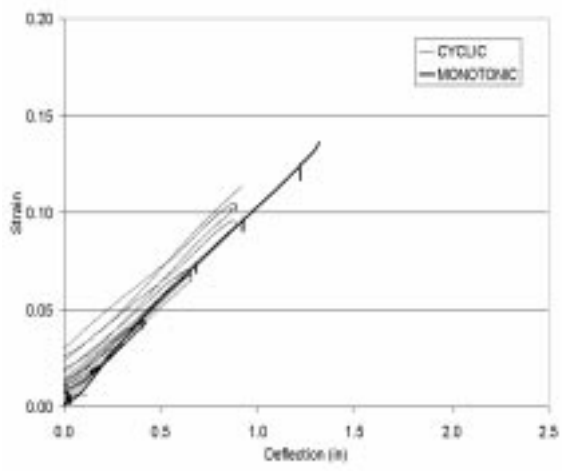

Figure 32. Strain demand in MC-arm at the high flexure region. Monotonic versus Cyclic Behaviour.

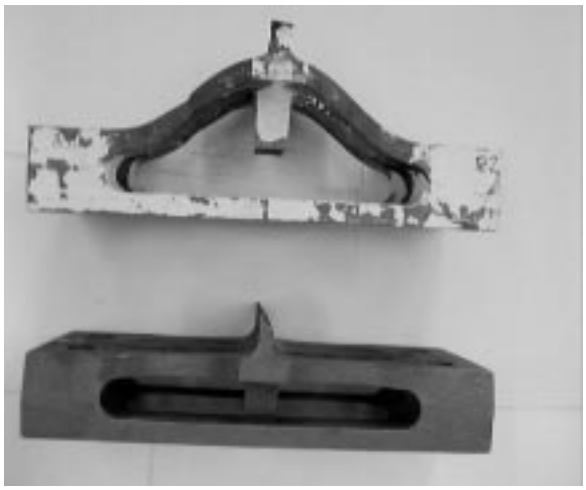

Figure 33. Deformed MC-Base under monotonic loading and undeformed MC-Base

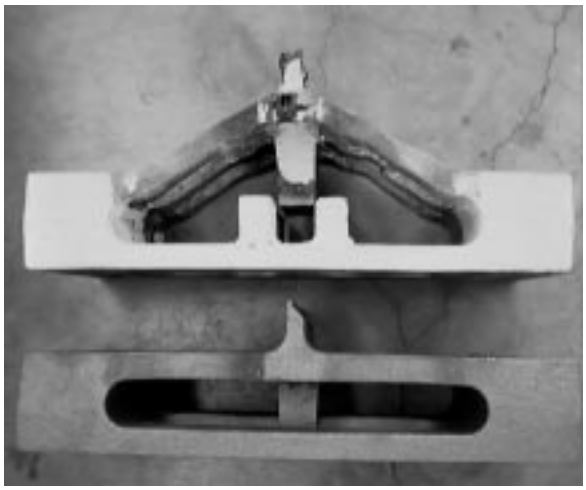

Figure 34. Deformed MC-Base under cyclic loading and undeformed MC-Base

- Bolt force increase is small (See Fig. 35).
- Bolt moment (curvature) is small (See Fig. 36).

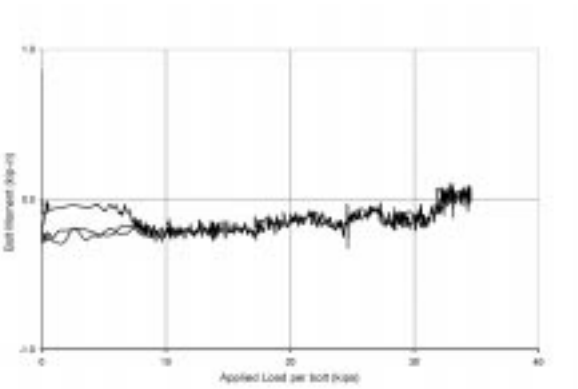

Figure 35. MC Base typical bolt head moment

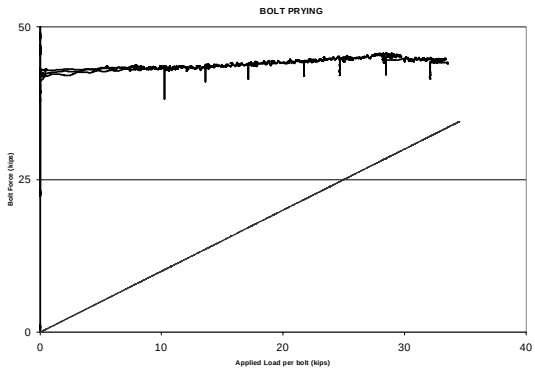

Figure 36. MC Base bolt prying plot

Figure 37. Fracture Plane of MC tested monotonically.

Figure 38. Fracture plane in the middle arm, necking in the outer arms of MC tested cyclically.

A.2.b MC-NoBase

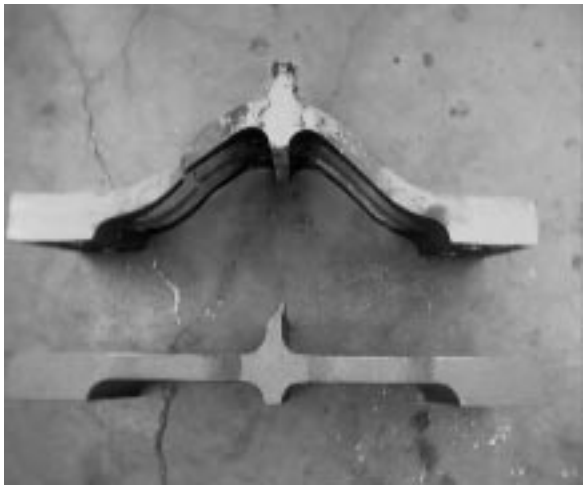

Figure 39. Deformed MC-Base under monotonic loading and undeformed MC-Base

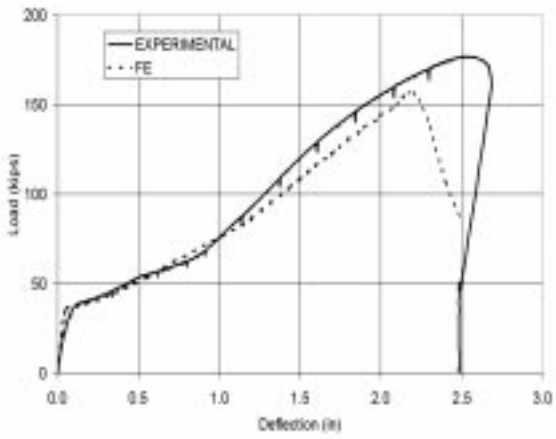

Figure 40. MC-NoBase Load Deflection. Experimental versus FE.

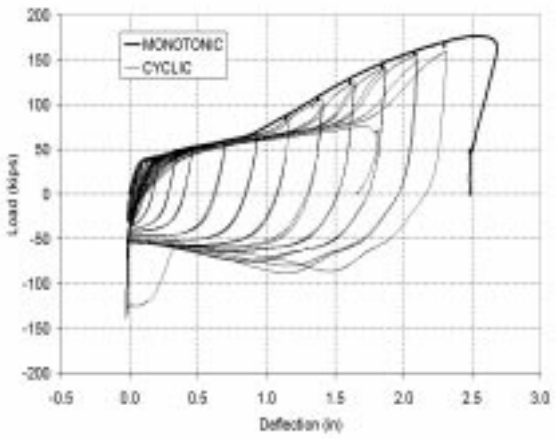

Figure 41. MC-NoBase Monotonic versus Cyclic Behaviour

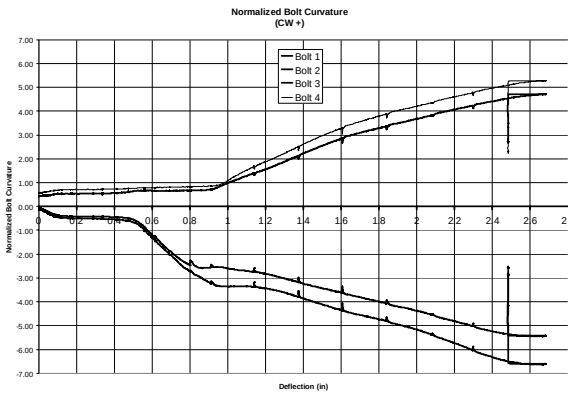

Figure 42. MC-NoBase Normalized bolt curvature

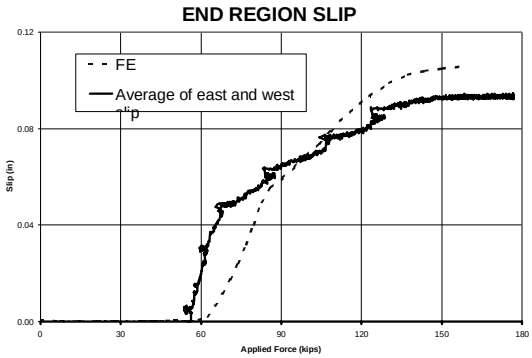

Figure 43.MC-NoBase end region slip

B. Findings of Modular Node for SMFs

The analytical model of the modular node was compared to the traditional (post-Northridge) and continuous joint. Important local behavior of the connections was evaluated within subassemblages. If not specified, all the studies were done with connection models of $\Omega = 2$.

It has been well understood that a weak panel zone causes distortion. The effect of panel zone (PZ) strength on local behavior was investigated for the modular node and compared to the traditional and continuous connection.

The variation in PZ strength was realized by changing the thickness of the PZ. Figure 44 shows the transition from strong PZ to weak PZ connections. For $\Omega \leq 1.0$, the energy dissipated by the PZ is a small percentage of the total, approximately 10%; for $\Omega > 1.7$, the majority (80% or more) is dissipated in the PZ; $\Omega > 2.0$ produces 90% PZ energy dissipation. In between ($\Omega = 1$ Ð 1.7), a rapid transition region exists. As shown in Figure 45, the curvature of the column flange converges to stable values for modular nodes with extremely strong or extremely weak PZs. A transition zone exists in between where column flange curvature changes with PZ strength.

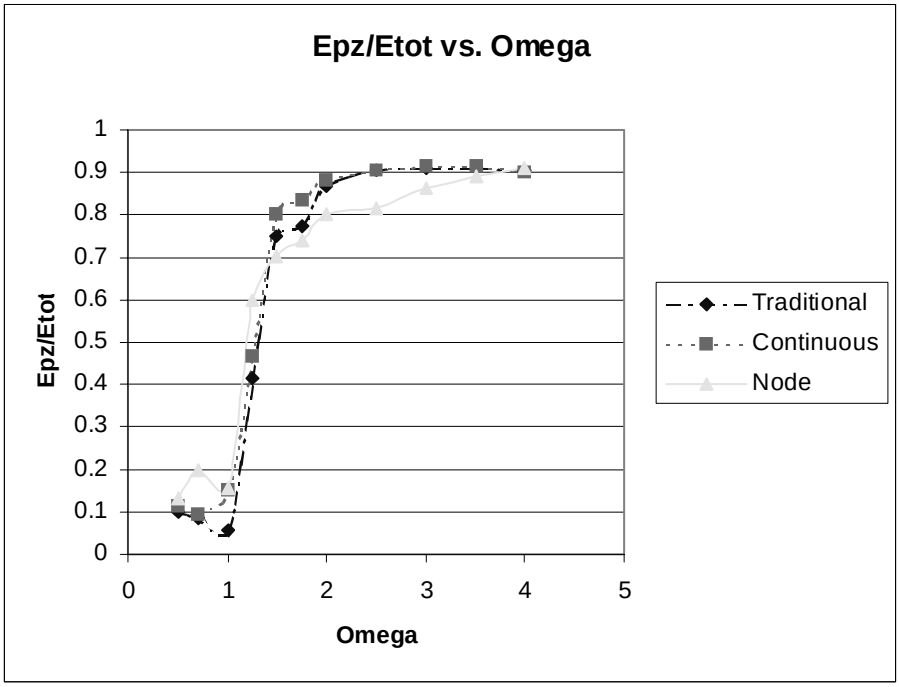

Figure 44. PZ energy dissipation percentage vs. omega.

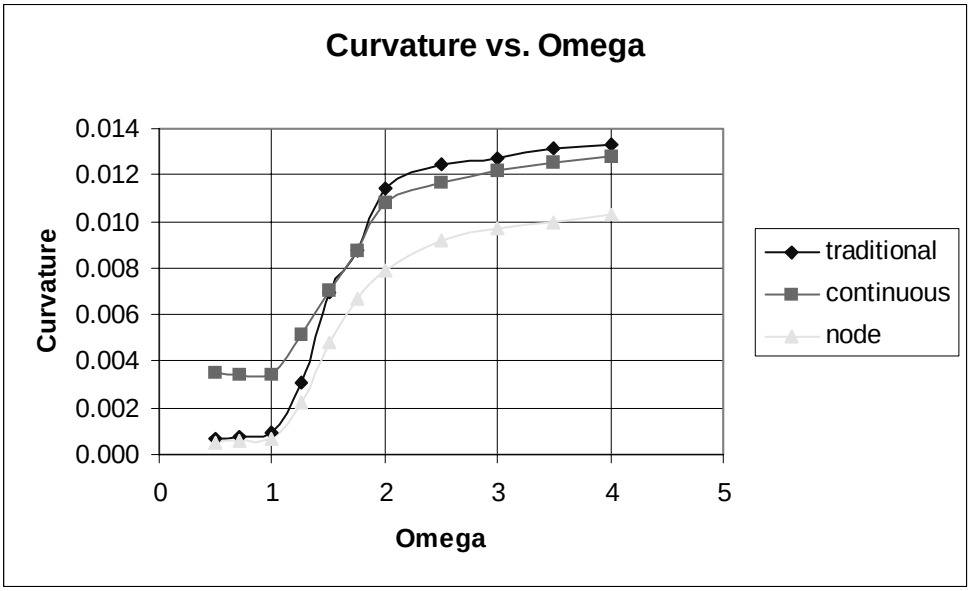

Figure 45. Curvature vs. omega for node.

B.1.a Comparison of Traditional Connection and PZ modular node

The condition of similar global behavior, i.e. load vs. story drift, is enforced. Figure 45 shows a comparison of column flange curvature at the beam flange interface, for a modular node, continuous and traditional connection with $\Omega = 2$. The values are plotted against the energy dissipated by the panel zone. The filleted cruciform feature of the modular node causes slightly less energy dissipation but a significant reduction in column curvature. It is noted that the column curvature endured by the traditional connection is not only over three times larger, it also occurs at a weld.

Figure 46 shows that the modular node greatly reduces the triaxiality across the beam flange in comparison to the traditional and continuous connection.

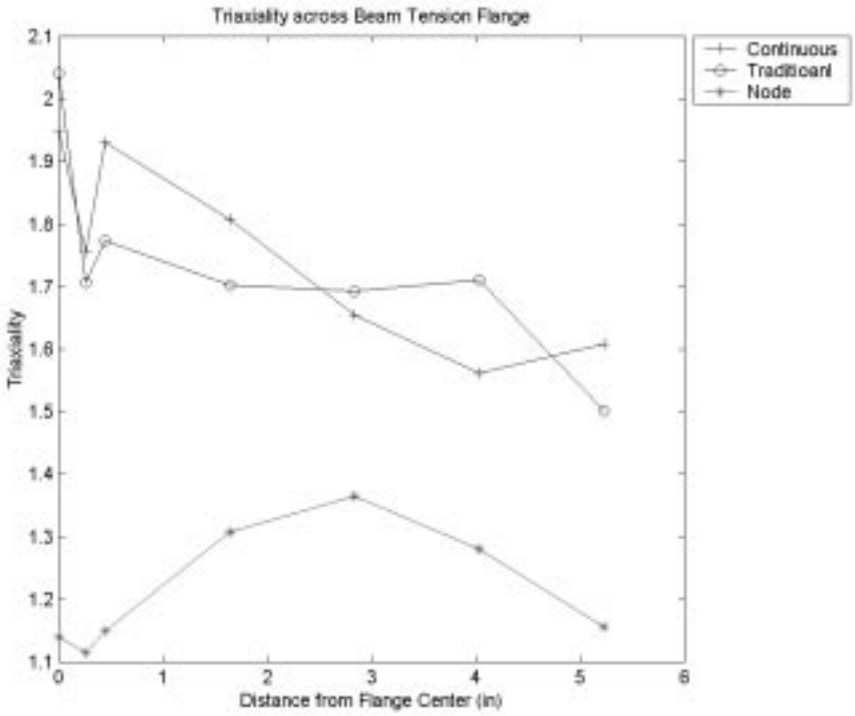

Figure 46. Triaxiality across the node beam flange.

B.1.b Effect of Geometric Parameters on Behavior of Modular Node

In this section, the effect of important geometric parameters on behaviors of modular node were investigated: (1) beam link slot length; (2) filleted cruciform size; (3) beam link length. Studies (1) and (2) are for a modular node with a beam link web. Study (3) is for a modular node without the beam link web.

(1) Effect of Beam Link Slot Length (PZ Modular Node): The effect of releasing the flange from the web, as is done in the slotted beam connection, is examined. Slots of different lengths are used as described in Table. The intent of this design modification is to lower the equivalent plastic strain in the column flange-beam flange juncture. Figure 47 shows that the effect of the slot on

global behavior is minimal. The equivalent plastic strain is lower for longer slot lengths, but the reduction reaches a point of diminishing return at lengths greater than 6.5" (see Figure 48, 49).

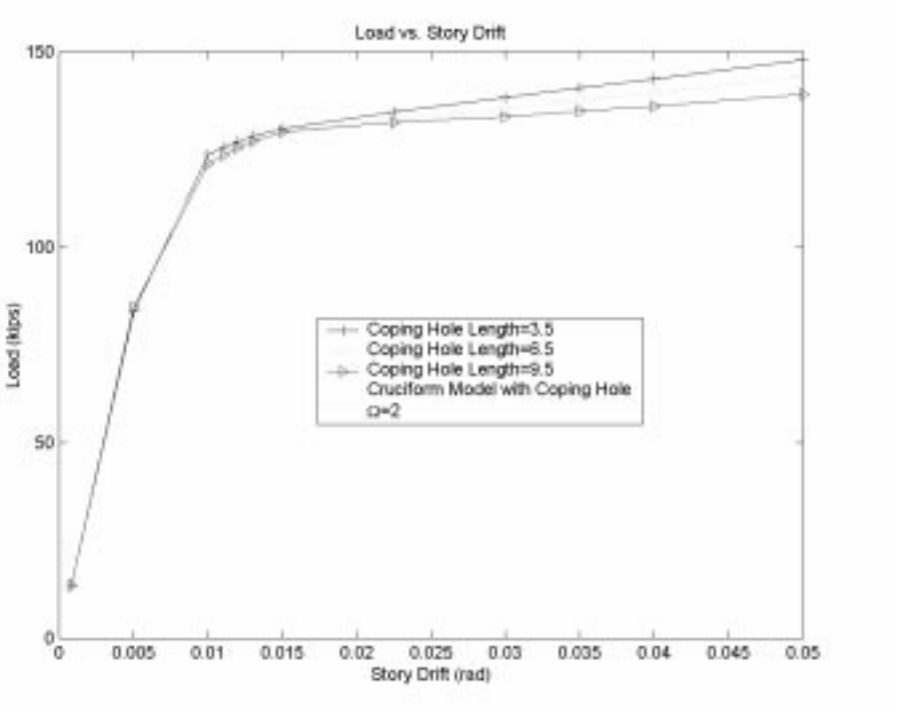

Figure 47. Global behavior for models with different length of coping hole.

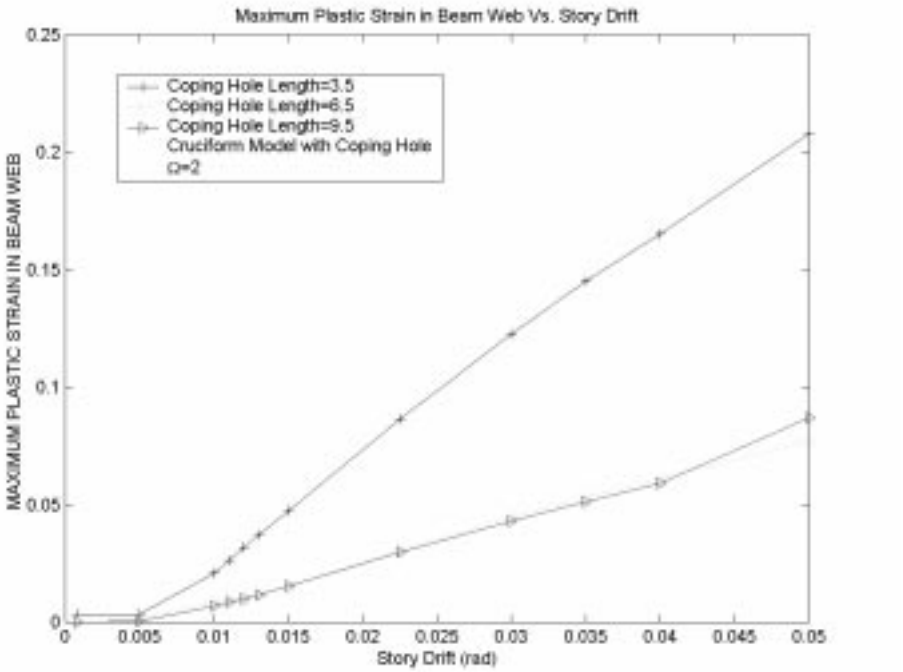

Figure 48. Maximum equivalent plastic strain in beam web comparison.

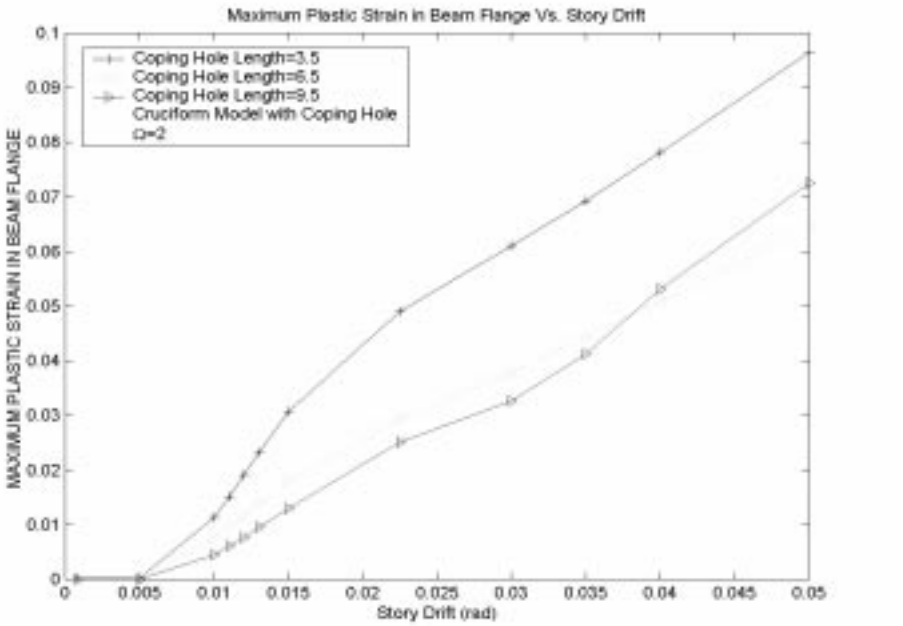

Figure 49. Maximum equivalent plastic strain in beam flange comparison.

The slotted web connection reduced the maximum equivalent plastic strain at beam link web. But according the later analyze, the modular node without beam link web completely eliminated

the equivalent plastic at beam link web. So the slotted web was not included in the final design of the PZ dissipator.

(2) Effect of Filleted Cruciform Size: The size of the fillet associated with the cruciform feature was examined. Figure 50 indicates that the fillet size does not significantly change the stiffness or strength of the PZ. Figure 51 shows that increasing the fillet size effectively reduces the column flange curvature. At a fillet size of 3", the curvature is effectively reduced to a minimal level. It is noted that the optimum value indicated is for the prototype members, i.e. W14x193 column and W30x99 beam.

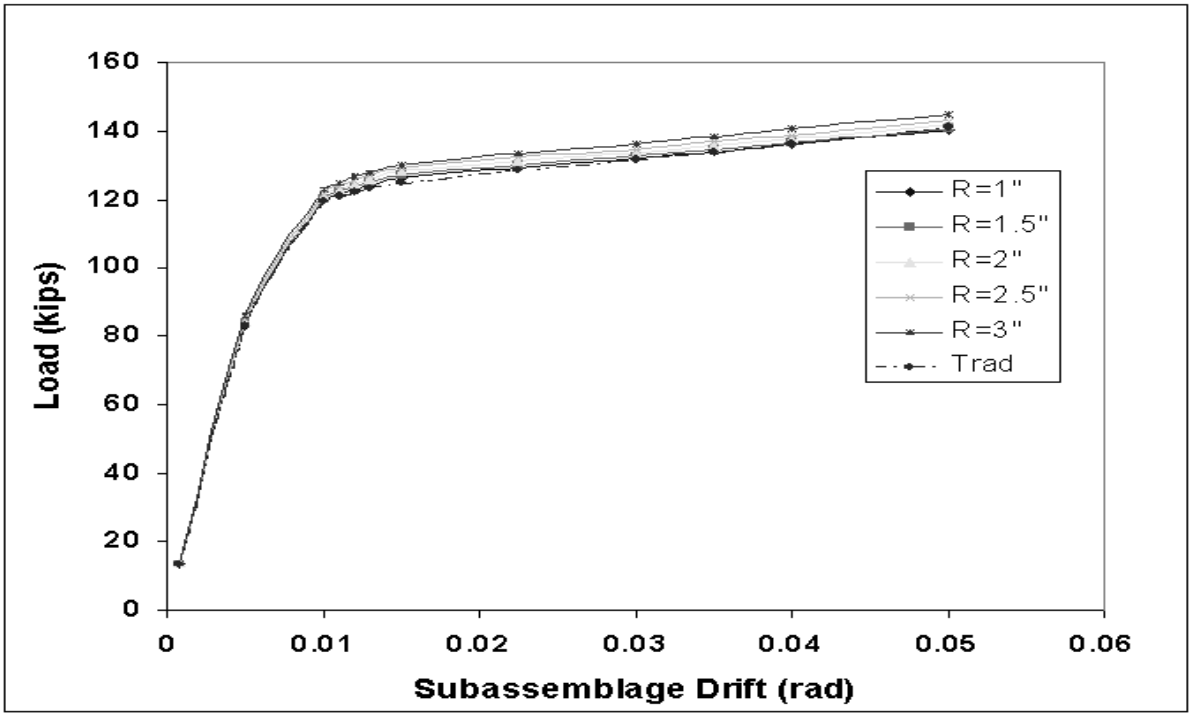

Figure 50. Global behavior comparison for nodes with different fillet cruciform size.

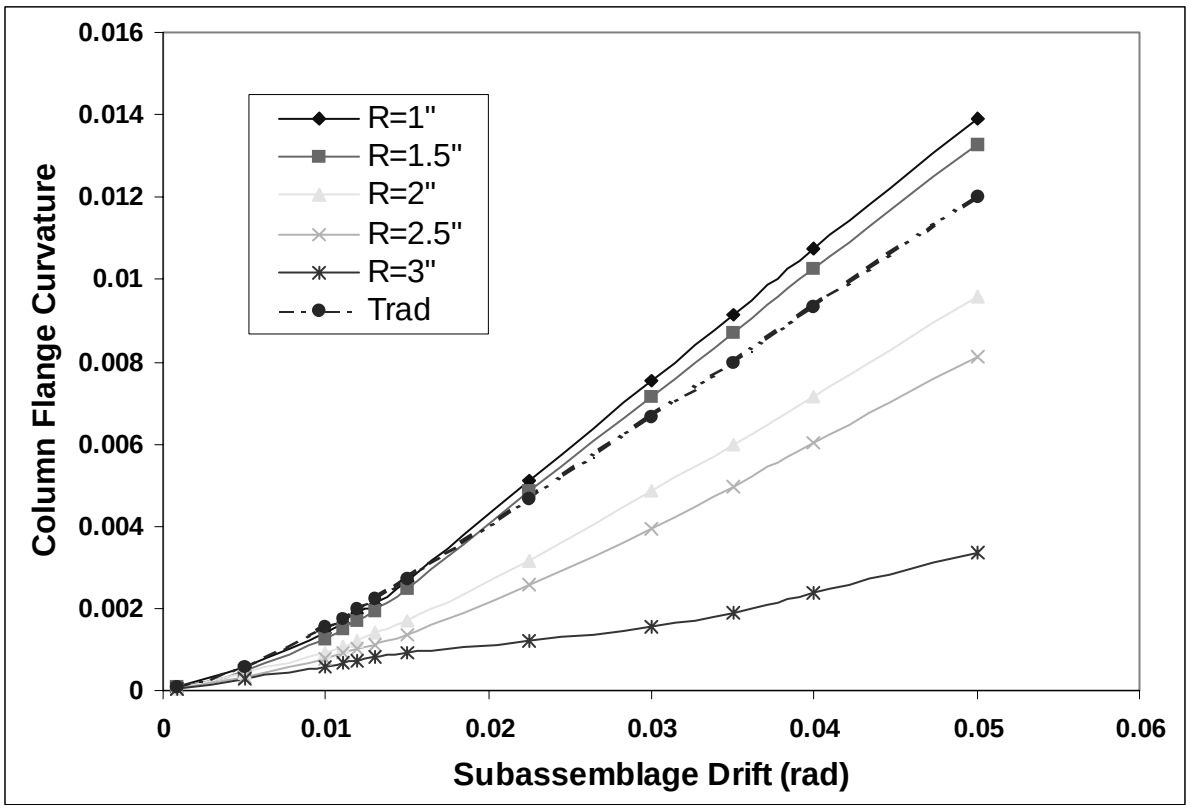

Figure 51. Curvature comparison for nodes with different fillet cruciform sizes.

(3) Effect of Beam Link Length for PZ Dissipator: The effect of the modular node beam link length was examined. Maximum equivalent plastic strain at the weld increases with the increase in beam link length (see Figure 52). As plastic strain at the weld is undesirable, it is necessary to modify the flange details of the beam link end. The design objective is to keep the weld and surrounding region elastic at up to a story drift of 0.05 radians. Figure 53 shows that the beam shear

will be more evenly distributed between tension flange and compression flange with the increasing of beam link length.

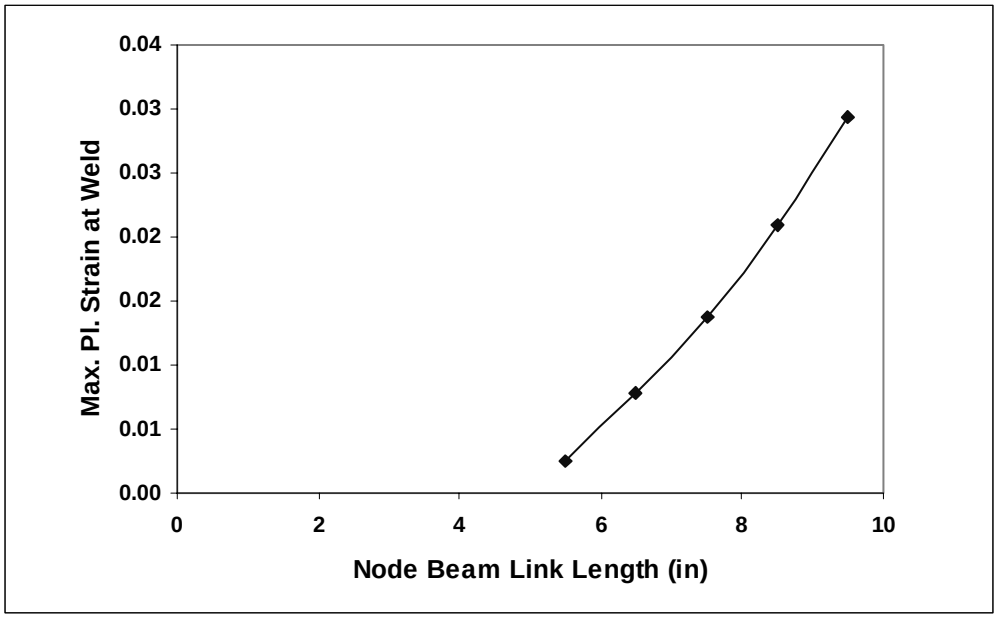

Figure 52. Maximum equivalent plastic strain at weld vs. beam link length.

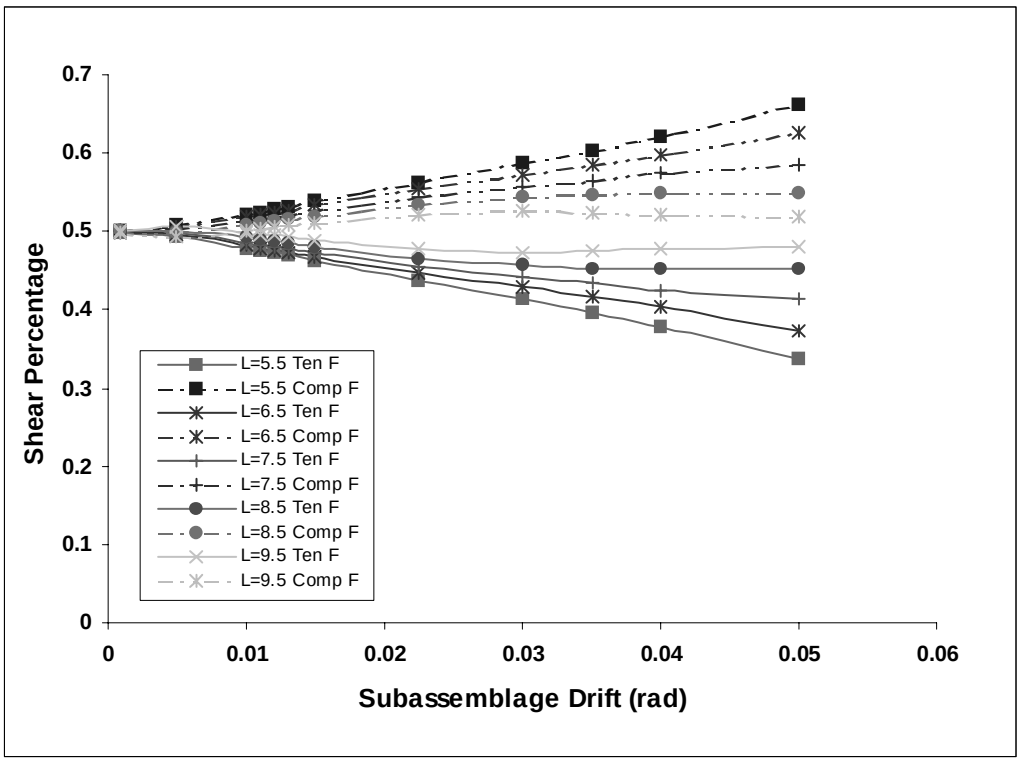

Figure 53. Shear distribution for different beam link lengths

B.1.c Features

In this section, four important features of the PZ dissipator modular node are investigated: (1) beam link web; (2) beam link end web connector; (3) RBS in beam link flange; and (4) beam link flange stiffener.

(1) Shear Transfer for Modular Node with and without Beam Link Web: During the research, the beam web region of the node was found to be detrimental to the performance of panel zone. As the beam flange region of the node by itself can sustain the beam shear, model of the node without a beam web was created for evaluation. It is found that the beam shear ratio was greatly lowered and the vertical stress was evenly distributed in the beam web for this configuration (See Figure 54).

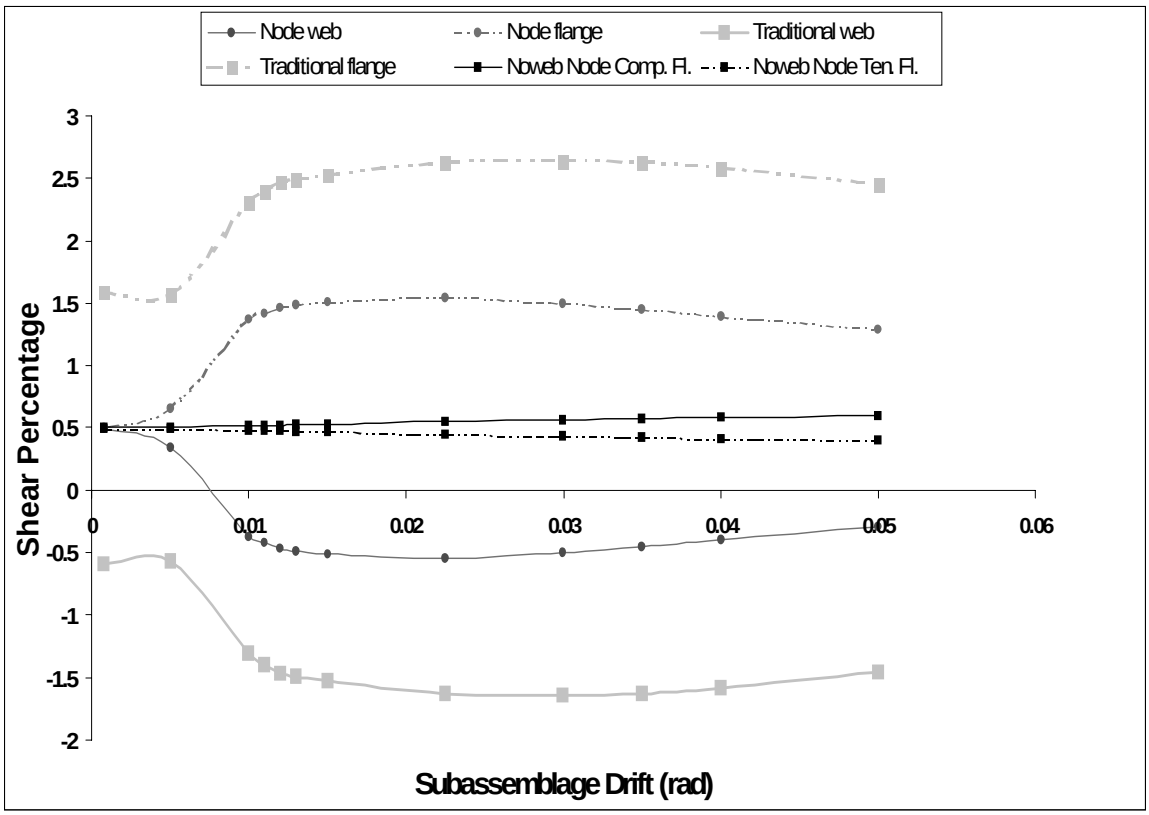

Figure 54. Carried beam shear percentage vs. story drift.

(2) Node Beam Link End Detail Study: Several different configurations for the node beam link details were examined. Figure 55 indicates that the reduced flange detail was not effective in reducing the maximum equivalent plastic strain at the weld, in fact the maximum equivalent plastic strain increased. However, the web connector detail successfully eliminated the maximum equivalent plastic strain at the weld region.

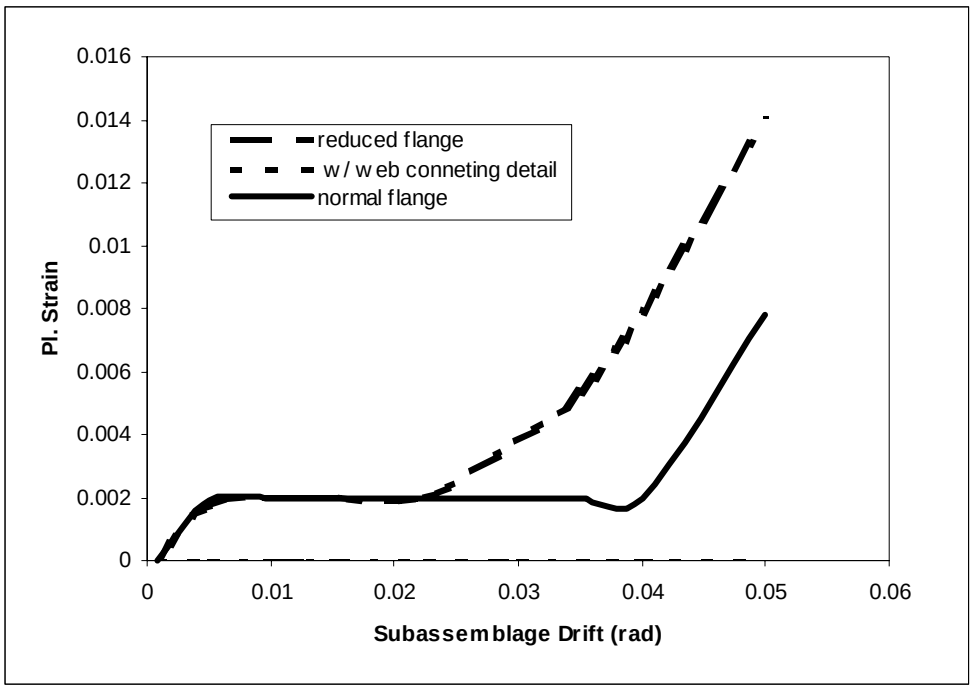

Figure 55. Maximum equivalent plastic strain at weld vs. story drift.

(3) Effect of Introducing RBS in Modular Node: The RBS concept has been incorporated to modular node. Figure 56 shows that the maximum equivalent plastic strain at the k-region was reduced by the addition of a RBS.

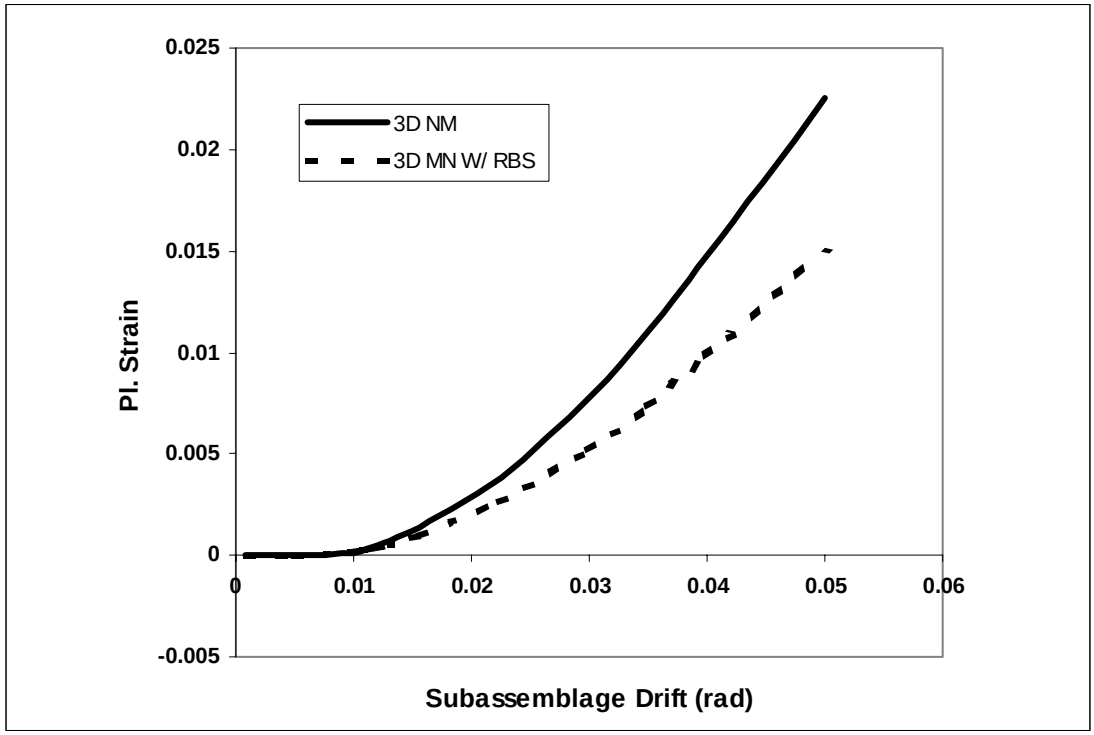

Figure 56. Maximum equivalent plastic strain at k-region vs. story drift.

(4) Node Beam Link Flange Stiffener Study: High normal stress was found to occur in the weld region of the PZ modular node (See Figure 57). The high stress occurs due to local bending of the beam link tension flange superimposed on the overall section bending stress. In order to minimize the stress demand at the weld, flange stiffeners were introduced to beam link to stabilize the flange (See Figure 58). The tensile stress at the weld region was reduced from 42 ksi to 25 ksi (See Figure 59), which is the nominal value anticipated due to the beam flexure alone.

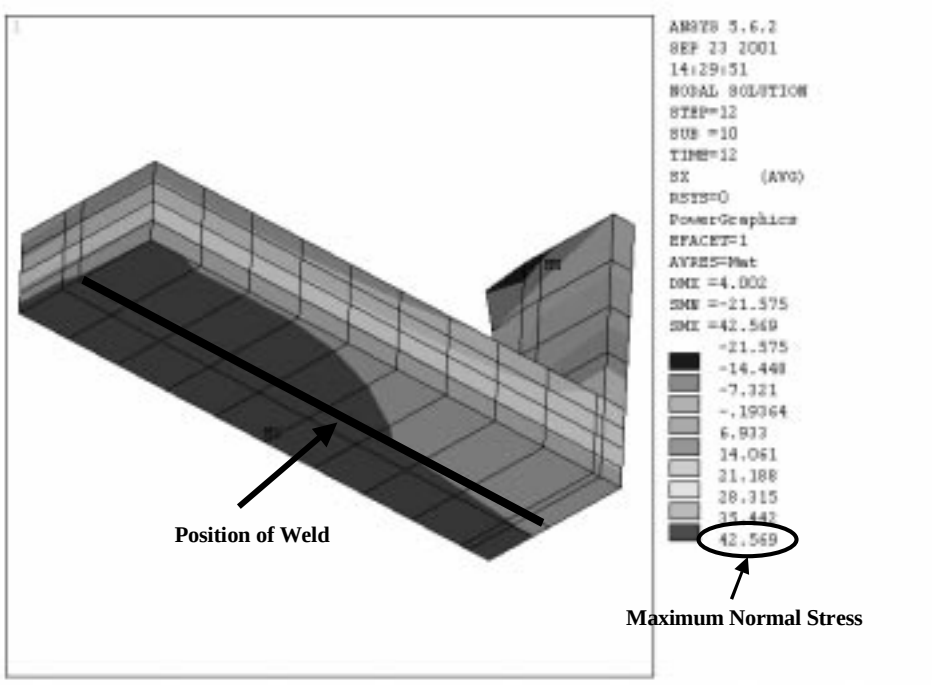

Figure 57. Normal stress at weld for node without flange stiffener.

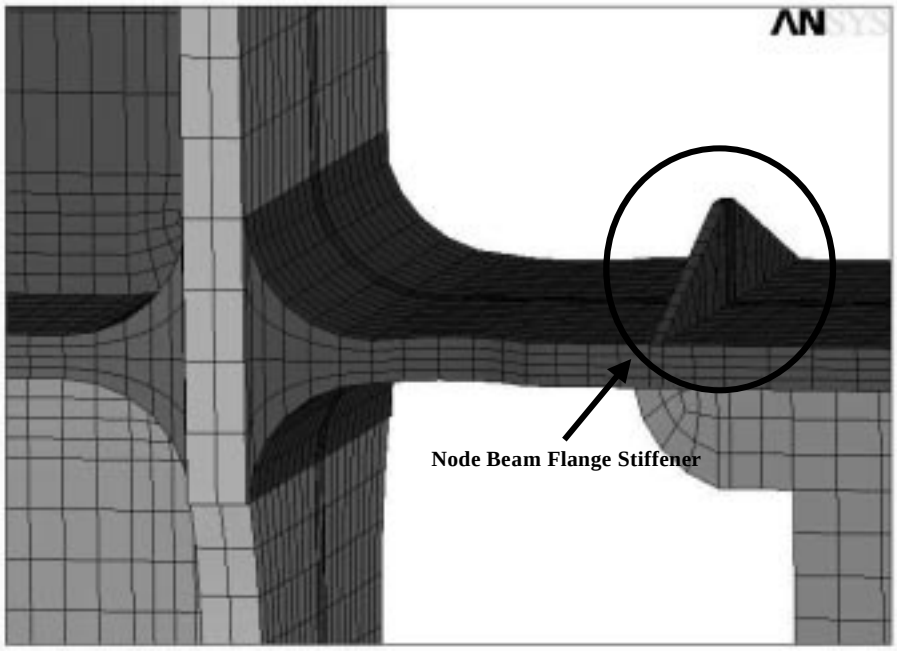

Figure 58. Configuration detail for flange stiffener.

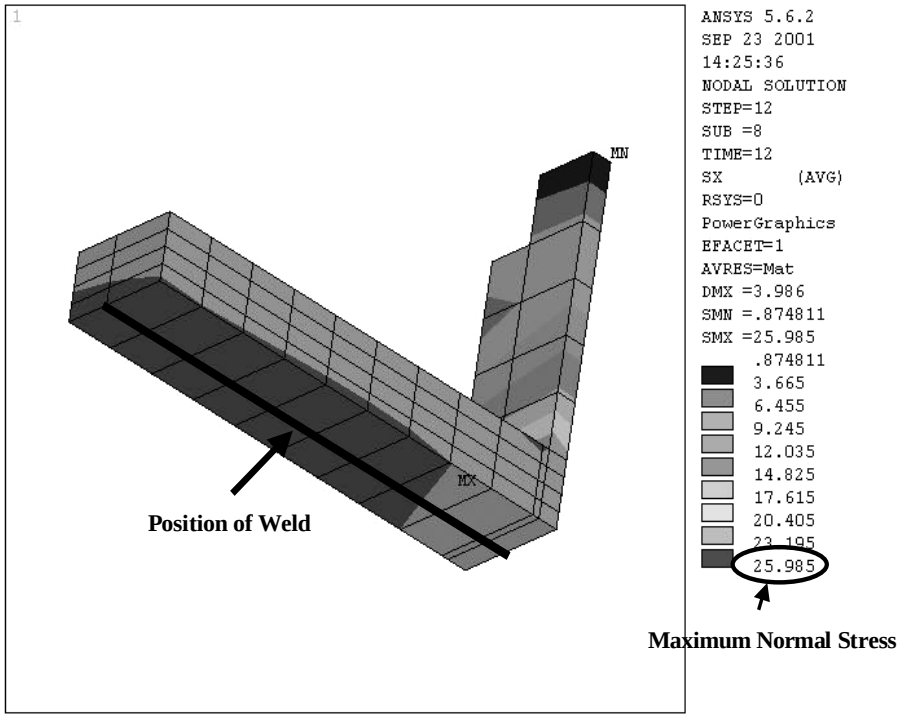

Figure 59. Normal stress at weld for node with flange stiffener.